X-ray Pulsar/Starlight Doppler Deeply-integrated Navigation Method

Yidi Wang, Wei Zheng and Dapeng Zhang

(*College of Aerospace Science and Engineering, National University of Defence Technology, Changsha, China*)
(E-mail: wangyidi_nav@163.com)

An X-ray pulsar/starlight Doppler deeply-integrated navigation method is proposed in this paper. A starlight Doppler measurement-aided phase propagation model, which can remove the orbital effect within the recorded photon Time Of Arrivals (TOAs), is derived, and guarantees that the pulse phase can be extracted from the converted photon TOAs using computationally efficient methods. Some simulations are performed by a hardware-in-loop system to verify the performance of the integrated pulse phase estimation method as well as of the integrated navigation method. The integrated pulse phase estimation method could achieve an estimation performance similar to the existing method for orbiting vehicles at the cost of much less computational complexity, is capable of handling the signals of millisecond pulsars, and is applicable to various vehicles. In addition, the proposed integrated navigation method could provide reliable positioning results for various vehicles.

1. INTRODUCTION.   In order to minimise the support of the ground-based tracking system and to enhance the survivability of vehicles facing a hostile environment, space vehicles are expected to be capable of handling some ordinary but necessary tasks such as autonomous navigation (Yang et al., 2014). Currently, Earth-orbiting vehicles with orbital altitudes of lower than 3000 km can implement autonomous navigation by employing Global Navigation Satellite Systems (GNSS). Unfortunately, GNSS is difficult to employ by Earth-orbiting vehicles orbiting at orbits higher than 3000 km, because the intensity of the GNSS signals rapidly decays as the orbital altitude of the client vehicle increases (Ning and Fang, 2007). Consequently, it is meaningful to develop an autonomous navigation system for those types of vehicles.

X-ray pulsar-based Navigation (XNAV) is a good choice for these vehicles. Pulsars are "dead" stars that spin and provide radiation with highly-stable periodicities (Lyne and Craham-Smith, 2012). From the navigation perspective, X-ray radiation, one type of pulsar

radiation, is recommended, as it is of high energy and could minimise the size of the sensor. The concept of XNAV was originally introduced in 1981, and has experienced a rapid growth over the past 30 years. The United States has performed a series of programs concerning XNAV since 1993. It is worth noting that the National Aeronautics and Space Administration (NASA) published its study on XNAV and announced a test of the navigation system on the International Space Station (ISS) in 2016 (Winternitz et al., 2015). Not only did the United States reveal its study on XNAV, but China, the European Space Agency, and the Max Planck Institute have drawn attention to XNAV (Wang et al., 2013; 2014; Sala et al., 2004; Becker et al., 2013). Currently, the building of XNAV is approaching completion but a few issues need to be further analysed.

XNAV operates by comparing the pulse Time Of Arrival (TOA) calculated at the vehicle with the pulse TOA at the Solar System Barycentre (SSB) predicted by the pulsar timing model. The discrepancy between the two pulse TOAs indicates the distance between the vehicle and the SSB, and can provide the positioning reference information for vehicles (Sheikh et al., 2006). How to effectively calculate the pulse TOA for orbiting vehicles is an important issue. Although the pulsar signal is assumed to be a form of pulse, in practice, a vehicle can merely record a series of discrete photon TOAs instead of continuous pulses, as the signal is extremely weak. Thus, a pulse TOA has to be extracted from the recorded photon TOAs, requiring solving of a stochastic signal processing problem. If the vehicle is assumed to be stationary or performing a uniform linear motion at a known velocity (i.e. the frequency of the received signal is constant), the pulse TOA can be calculated using two well-developed types of methods. The first is the epoch folding method, which first recovers an empirical profile using the photon TOAs and calculates the pulse TOA by comparing the empirical profile with the template, a profile with a high signal to noise ratio, built by the astronomical data, and the second is the direct use of photon TOAs, which calculates the pulse TOA by maximising a likelihood function derived based on the nonhomogeneous Poisson process describing the photon TOAs (Emadzadeh and Speyer, 2011). However, in practice, the vehicles are normally performing orbital motions, causing the frequency of the received pulsar signal to vary with time and the failure of the aforementioned methods.

In order to cope with the problem, Golshan and Sheikh (2007) proposed a pulse phase tracking algorithm. The time-varying frequency of the received pulsar signal is approximated as an interval-wise constant model that divides an observation period of a pulsar into intervals over each of which the orbital motion of the vehicle could be assumed as a uniform linear motion. A two-dimensional Maximum Likelihood Estimator (MLE) is derived to estimate the initial phase as well as the frequency at the start epoch of each interval, and is followed by a Digital Phase-Locked Loop (DPLL) tracking the variation of frequency between intervals next to each other. The duration of the divided interval is a key factor. If the duration is shorter than a certain threshold that depends on the flux of a pulsar, the output of the MLE would diverge from the Cramér-Rao bound (CRB) and become unreliable (Tran et al., 2014). On the other hand, if the duration is too long then the vehicle cannot be assumed to perform a linear motion within each interval. For young pulsars with large fluxes, such as the Crab pulsar, the thresholds are less than 1 s, and it is easy to select an appropriate duration of divided interval. For the millisecond pulsars with faint fluxes, such as PSR B1821-24, the thresholds are around 100 s, resulting in the need for the divided interval to be longer than at least 100 s. There are few situations where a vehicle can be fiducially assumed to perform a uniform linear motion over 100 s. Thus, the pulse phase tracking algorithm is not suggested to cope with the signals of millisecond pulsars.

In Wang and Zheng (2016), we proposed a pulse phase estimation method using the orbital dynamics of the vehicle, which will be referred to as the linearized method in the remainder of the paper. The pulse phase propagation model is modified as a term of the position of the vehicle. As the position of the vehicle can be predicted by propagating the initial position and velocity of the vehicle, a linearized pulse phase propagation model, which is linearized around the predicted position, is derived. The linearized pulse phase propagation model separates the classical pulse phase propagation model into a predicted component and a polynomial component left to be estimated. The method does not divide the observation period into intervals and is capable of coping with the signals of millisecond pulsars. A multi-dimensional maximum likelihood estimator is applied to estimate all the coefficients of the polynomial and the pulse phase. Thus, the computational burden of the method is a big issue, as the order of the polynomial would be at least two for Earth-orbiting vehicles. Although the parallel computation technique was employed to address the problem, the technique still brings a strict requirement on the satellite-borne computer. In addition, the linearized method is not applicable to vehicles orbiting in low orbits, as the linearization error would greatly accumulate as the orbital altitude decreased.

To overcome the shortcomings of the linearized method, we propose an X-ray pulsar/starlight Doppler deeply-integrated navigation method in this paper. The starlight Doppler measurement refers to the velocity of a vehicle towards an observed star and can be obtained by investigating the Doppler shift of the starlight using a spectrometer (Liu et al., 2015). Its accuracy ranges from 0·01 m/s to 1 m/s. Although it is well documented that the six-dimensional states of a vehicle, including three positions and three velocities along each coordinate axis, cannot be completely estimated by processing only the starlight Doppler measurements (Yim, 2002), the velocity of the vehicle can be geometrically calculated by handling three starlight Doppler measurements. As the sampling period of the starlight Doppler measurement is much shorter than the observation period of a pulsar, the velocity of the vehicle can be introduced into the classical pulse phase propagation model to roughly remove the orbital effect within the recorded photon TOAs, bringing in a starlight Doppler-aided pulse propagation model. An integrated pulse phase estimation method is derived. The method is accomplished by the following procedure: (1) geometrical calculation of the velocity of vehicle, (2) removal of the orbital effect within the recorded photon TOAs, and (3) estimation of the pulse phase. As the computational complexity of the epoch folding method is much less than that of the direct use of photon TOAs, the epoch folding method is employed to estimate the pulse phase. The proposed integrated pulse phase estimation method does not divide the observation period of a pulsar into intervals and does not need a linearization or a multi-parameter estimation, so it can handle the signals of millisecond pulsars, is computationally efficient, and has an application field wider than the linearization method.

The proposed deeply-integrated navigation method is quite different from the existing integrated navigation method using X-ray pulsars and starlight Doppler. The existing method is a loosely-coupled integration that directly uses the starlight Doppler measurement and the pulse TOA to estimate the position of the vehicle using Kalman filters. In contrast, the integration of the proposed method goes deeper, as the starlight Doppler measurement is used to aid the pulse phase estimation, and only the pulse TOA is employed to estimate the position of the vehicle.

The rest of the paper proceeds as follows. Section 2 designs the proposed integrated navigation system and compares the information fusion within the proposed system and
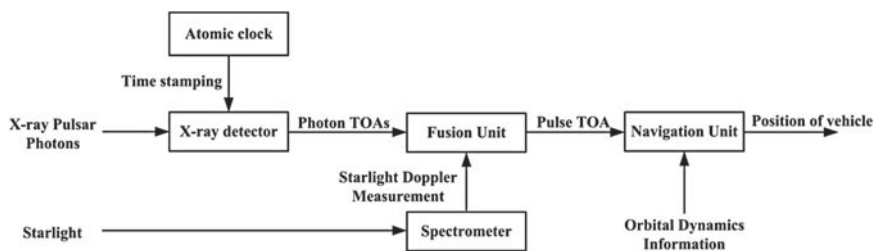
Figure 1.   Information flow of the proposed integrated navigation system.
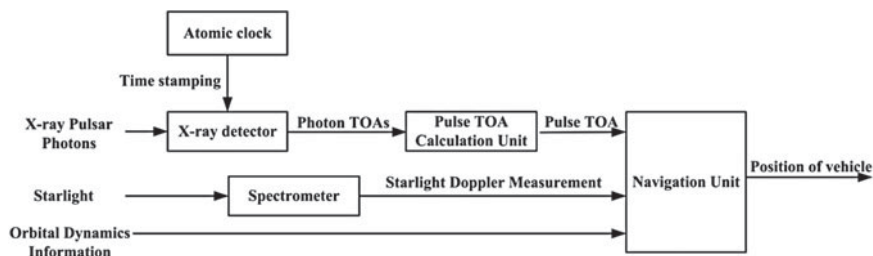

Figure 2.   Information flow of the existing integrated navigation system.

within the existing integrated navigation system. Section 3 briefly reviews the works related to the pulse phase estimation, laying the foundation for further investigations. Section 4 shows how to integrate the starlight Doppler measurement into the pulse phase estimation in detail. Some simulations via a hardware-in-loop system are performed in Section 5 to verify the proposed method.

2.   OVERALL DESIGN OF THE INTEGRATED NAVIGATION SYSTEM.   Figure 1 shows the information flow of the proposed integrated navigation system. The system contains the following units: 1) X-ray detectors detecting the X-ray pulsar photons; 2) Atomic clocks providing the time stamp of the pulsar photons; 3) Spectrometer providing the starlight Doppler measurement by analysing the spectrum of starlight; 4) Fusion unit fusing the starlight Doppler measurement and the photon TOAs to produce the pulse TOA; and 5) Navigation unit estimating the position of the vehicle by fusing the pulse TOA and the orbital dynamics information of the vehicle.

For comparison, Figure 2 provides the information flow of the existing integrated navigation system. The pulse TOA is independently calculated, and is fused with the starlight Doppler measurement and the orbital dynamics information to estimate the position of the vehicle in the navigation unit.

As the fusion unit is the key portion in the proposed integrated navigation system, we will focus on its design in the following sections.

3.   WORKS RELATED TO THE PULSE PHASE ESTIMATION.   Before the detailed design of the fusion unit, we briefly review the works related to the pulse phase estimation.

3.1.   *X-ray pulsar signal model for orbiting vehicles.*   The process for a vehicle to record a series of X-ray photon TOAs can be modelled as a nonhomogeneous Poisson

process with a periodic rate function $\lambda(t) \geq 0$. $\lambda(t)$ indicates the aggregate rate of photons from pulsar and background, and is of the form (Emadzadeh and Speyer, 2010a)

$$\lambda(t) = \alpha h(\phi_{\text{det}}(t)) + \beta \tag{1}$$

where $h(\cdot)$ is the periodic pulsar profile, $\phi_{\text{det}}(t)$ is the detected phase, and α and β are the detected rate constant of the pulsar and of the background respectively.

Taking the orbital motion of the vehicle into consideration, $\phi_{\text{det}}(t)$ can be modelled as

$$\phi_{\text{det}}(t) = \phi_0 + f_s(t - t_0) + \frac{f_s}{c}\int_{t_0}^{t} v(\tau)d\tau \tag{2}$$

where ϕ_0 is the detected phase at initial time t_0, f_s is the intrinsic frequency of the pulsar, c is the speed of light, and v is the velocity of the vehicle towards the pulsar.

When the vehicle has a velocity of v and the direction vector of the pulsar is n, Equation (2) can be rewritten as

$$\phi_{\text{det}}(t) = \phi_0 + f_s(t - t_0) + \frac{f_s}{c}\int_{t_0}^{t} n \cdot v(\tau)d\tau \tag{3}$$

3.2. *Epoch folding.*   Epoch folding that could recover the pulse profile from a series of recorded photon TOAs has been widely applied in the astronomy field.

Suppose an observation period lasting for T_{obs} seconds consists of N_p periods of the received signal, P. P can be further divided into N_b bins, the size of which is T_b seconds. Epoch folding proceeds as follows. Firstly, all the photons are folded back into the first period according to their TOAs. Then, the photons collected in each bin are counted. Finally, an empirical profile can be recovered by normalising the computed photon counts.

The empirical profile in the ith bin $i \in [1, N_b]$, $\tilde{\lambda}(T_i)$, can be described by (Emadzadeh and Speyer, 2010b)

$$\tilde{\lambda}(T_i) = \lambda(T_i, \phi_0) + n(T_i) \tag{4}$$

where $\lambda(T_i, \phi_0)$ is the template with an initial phase ϕ_0 and $n(T_i)$ is the epoch folding noise.

When the empirical profile is built, ϕ_0 can be estimated by comparing the template and the empirical profile by some computationally efficient methods such as the cross-correlation method or the fast near-maximum likelihood estimator (Rinauro et al., 2013). Figure 3 describes the whole process of the epoch folding. It is obvious that the epoch folding method relies on the assumption that the period of the signal is constant. Thus, the classical epoch folding method cannot be directly employed by orbiting vehicles, as the period of the received signal of those vehicles would vary with time.

3.3. *Linearized method.*   In Wang and Zheng (2016), we rewrote the integral term on the right side of Equation (3) as

$$\int_{t_0}^{t} n \cdot v(\tau)d\tau = n \cdot r(t) - n \cdot r(t_0) \tag{5}$$

where $r(\cdot)$ is the position of the vehicle.

As $r(\cdot)$ can be expressed as the sum of the position predicted by the orbital dynamics of vehicle $\tilde{r}(\cdot)$ and the error within $\tilde{r}(\cdot)$, $\delta r(\cdot)$, and the transition matrix that connects
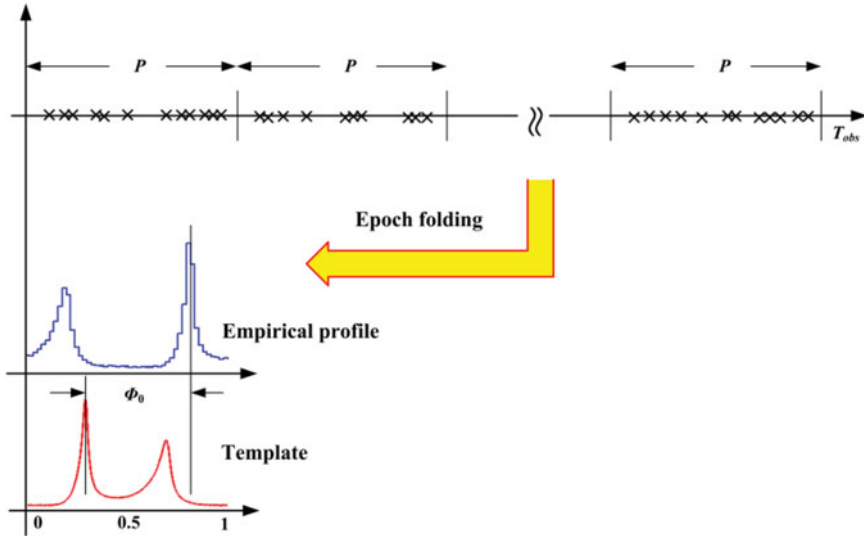
Figure 3.   Diagram of the epoch folding.

the $\delta r\,(\cdot)$s can be written in a polynomial form, we have the linearized phase propagation model of

$$\phi_{\text{det}}\,(t) = \phi_0 + f_s\,(t - t_0) + \sum_{k=1}^{\infty} f_{dy}^{(k)}\,(t - t_0)^k + \frac{f_s}{c}\boldsymbol{n} \cdot [\tilde{\boldsymbol{r}}\,(t) - \tilde{\boldsymbol{r}}\,(t_0)] \tag{6}$$

where $f_{dy}^{(k)}$ is the coefficients of the polynomial that need to be estimated.

For Earth-orbiting vehicles, Equation (6) can be rewritten as

$$\phi_{\text{det}}\,(t) = \phi_0 + f_s\,(t - t_0) + \sum_{k=1}^{\infty} f_{dy}^{(k)}\,(t - t_0)^k + \frac{f_s}{c}\boldsymbol{n} \cdot \left[\tilde{\boldsymbol{r}}_{SC/E}\,(t) - \tilde{\boldsymbol{r}}_{SC/E}\,(t_0)\right]$$

$$+ \frac{f_s}{c}\boldsymbol{n} \cdot [\tilde{\boldsymbol{r}}_E\,(t) - \tilde{\boldsymbol{r}}_E\,(t_0)] \tag{7}$$

where $\tilde{\boldsymbol{r}}_{SC/E}\,(\cdot)$ is the position of the vehicle with respect to the Earth and $\tilde{\boldsymbol{r}}_E\,(\cdot)$ is the position of the Earth with respect to the SSB that could be provided by the Jet Propulsion Laboratory (JPL) ephemeris such as DE405 or DE421.

4. INTEGRATED PULSE PHASE ESTIMATION METHOD. Taking an Earth-orbiting vehicle as an example, this section will illustrate how to estimate the velocity of the vehicle using starlight Doppler measurements and to estimate the pulse phase using the estimated velocity. Although the investigation is for Earth-orbiting vehicles, the methods can be readily extended for deep space explorers.

Figure 4 gives a sketch of the integrated pulse phase estimation method. The proposed method needs three starlight Doppler measurements to calculate the velocity of the vehicle within an observation period of a pulsar.
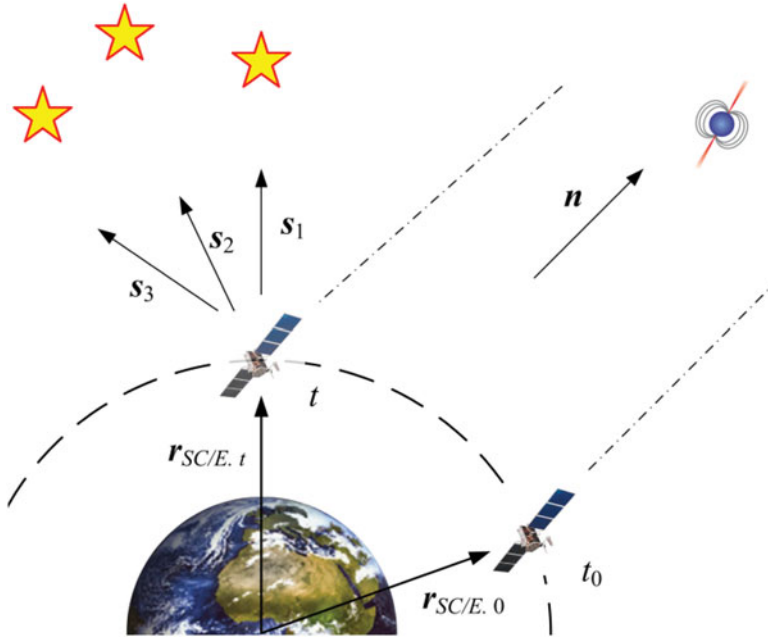
Figure 4.   Graphic description of the integrated pulse phase estimation method.

4.1.   *Velocity acquisition via starlight Doppler measurements.*   Assuming a spectrometer measures the Doppler frequency shift of the ith star ($i = 1, 2, 3, ...$) and obtains the velocity of the vehicle towards the ith star, v_i, the measurement model for velocity acquisition is (Liu et al., 2015)

$$v_i = s_i^T v_{SC/E} + s_i^T v_E - v_{s,i} + \zeta_i \tag{8}$$

where $s_i \in \mathbb{R}^{3 \times 1}$ is the direction vector of the ith star, $v_{s,i}$ is the radial velocity of the ith star, $v_{SC/E}$ is the velocity of the vehicle relative to the Earth, v_E is the velocity of the Earth that could also be provided by DE405, and ζ_i is the measurement noise.

Assuming three stars are observed, Equation (8) can be rewritten in a matrix form of

$$Z = S \left(v_{SC/E} + v_E \right) + Z_s + \zeta \tag{9}$$

where $Z = [v_1 \quad v_2 \quad v_3]^T$, $S = [s_1^T \quad s_2^T \quad s_3^T]^T$, $Z_s = [v_{s,1} \quad v_{s,2} \quad v_{s,3}]^T$,   and $\zeta = [\zeta_1 \quad \zeta_2 \quad \zeta_3]^T$.

Thus, $v_{SC/E}$ can be estimated by

$$\hat{v}_{SC/E} = \left(S^T R^{-1} S \right)^{-1} S^T R^{-1} \left(Z - Z_s \right) - v_E \tag{10}$$

where R is the covariance of ζ. The covariance of $\hat{v}_{SC/E}$ is $cov \left(\hat{v}_{SC/E} \right) = \left(S^T R^{-1} S \right)^{-1}$.

4.2. *Starlight Doppler measurement-aided phase propagation model.*

4.2.1. *Derivation.* In contrast to the way the linearization method modifies the integral term in Equation (3), in this subsection, we solve the integral term by numerically integrating rather than analytically solving it. For Earth-orbiting vehicles, we have

$$\int_{t_0}^{t} \mathbf{n}^T \mathbf{v}(\tau) d\tau = \int_{t_0}^{t} \mathbf{n}^T \mathbf{v}_{SC/E}(\tau) d\tau + \mathbf{n} \cdot [\tilde{\mathbf{r}}_E(t) - \tilde{\mathbf{r}}_E(t_0)] \tag{11}$$

As the second term on the right hand of Equation (11) is known, we focus on solving the first term. It is well known that $\int_{t_0}^{t} \mathbf{n}^T \mathbf{v}_{SC/E}(\tau) d\tau$ can be solved using the composite trapezoid formula (Hildebrand, 1974). Assuming the observation period $[t_0 \quad t]$ consists of N sampling periods of the starlight Doppler measurement, T_s, we have

$$\int_{t_0}^{t} \mathbf{n}^T \mathbf{v}_{SC/E}(\tau) d\tau \approx \frac{T_s}{2} \sum_{j=1}^{N-1} \left(\mathbf{n}^T \mathbf{v}_{SC/E,j} + \mathbf{n}^T \mathbf{v}_{SC/E,j+1} \right) \tag{12}$$

where $\mathbf{v}_{SC/E,j}$ is the true velocity of vehicle at the end epoch of the jth sampling period of the starlight Doppler measurement.

Given that the true velocity of the vehicle is unknown, we substitute the estimated velocity $\hat{\mathbf{v}}_{SC/E}$ into Equation (12), yielding

$$\int_{t_0}^{t} \mathbf{n}^T \mathbf{v}_{SC/E}(\tau) d\tau \approx \frac{T_s}{2} \sum_{j=1}^{N-1} \left(\mathbf{n}^T \hat{\mathbf{v}}_{SC/E,j} + \mathbf{n}^T \hat{\mathbf{v}}_{SC/E,j+1} + \mathbf{n}^T \boldsymbol{\xi}_j + \mathbf{n}^T \boldsymbol{\xi}_{j+1} \right) \tag{13}$$

where $\boldsymbol{\xi}_j$ is the error within $\hat{\mathbf{v}}_{SC/E,j}$ and can be modelled as a zero-mean Gaussian noise.

When N approaches infinity, we have

$$\frac{T_s}{2} \sum_{j=1}^{N-1} \left(\mathbf{n}^T \boldsymbol{\xi}_j + \mathbf{n}^T \boldsymbol{\xi}_{j+1} \right) \approx 0 \tag{14}$$

In practice, the sampling period of starlight Doppler measurement is in the order of a second and the observation period of a pulsar is in the order of hours. Thus, the assumption that N is approximated to be infinite readily holds in real space missions.

Substituting Equations (13) and (14) into Equation (3) yields

$$\phi_{\det}(t) = \phi_0 + f_s(t - t_0) + \frac{f_s T_s}{2c} \sum_{j=1}^{N-1} \left(\mathbf{n}^T \hat{\mathbf{v}}_{SC/E,j} + \mathbf{n}^T \hat{\mathbf{v}}_{SC/E,j+1} \right) + \frac{f_s}{c} \mathbf{n} \cdot [\tilde{\mathbf{r}}_E(t) - \tilde{\mathbf{r}}_E(t_0)] \tag{15}$$

Equation (15) could be used as the starlight Doppler measurement-aided phase propagation model, if the sampling period of starlight Doppler measurement is close to the difference between the recorded TOAs of photons next to each other. However, in practice, the sampling period of the starlight Doppler measurement is in the order of a second, but the difference between the TOAs of photons next to each other is usually shorter than the intrinsic period of a pulsar, which is usually in the order of a millisecond. This means there would be many photon TOAs that are not employed to estimate the pulse phase if Equation (15) were used as it would reduce the phase estimation accuracy. In order to introduce those

"lost" photon TOAs into the pulse phase estimation, we use linear interpolation to modify Equation (15).

When $t_p \in [jT_s \quad (j+1)\,T_s]$ the velocity of the vehicle at t_p can be approximated as a term of $\hat{\boldsymbol{v}}_{SC/E,j}$ and $\hat{\boldsymbol{v}}_{SC/E,j+1}$,

$$\boldsymbol{v}_p = \left(1 - \frac{t}{T_s}\right)\hat{\boldsymbol{v}}_{SC/E,j} + \frac{t}{T_s}\hat{\boldsymbol{v}}_{SC/E,j+1} \tag{16}$$

Then, we have

$$\phi_{\det}\left(t_p\right) = \phi_0 + f_s\left(t_p - t_0\right) + \frac{f_s T_s}{2c}\sum_{k=1}^{j-1}\left(\boldsymbol{n}^T\hat{\boldsymbol{v}}_{SC/E,k} + \boldsymbol{n}^T\hat{\boldsymbol{v}}_{SC/E,k+1}\right)$$

$$+ \frac{f_s}{2c}\left(t - jT_s\right)\left(\boldsymbol{n}^T\hat{\boldsymbol{v}}_{SC/E,j} + \boldsymbol{n}^T\boldsymbol{v}_p\right) + \frac{f_s}{c}\boldsymbol{n}\cdot\left[\tilde{\boldsymbol{r}}_E\left(t\right) - \tilde{\boldsymbol{r}}_E\left(t_0\right)\right] \tag{17}$$

In summary, the starlight Doppler measurement-aided phase propagation model is

$$\phi_{\det}\left(t\right) = \phi_0 + f_s\left(t - t_0\right) + \frac{f_s}{c}\boldsymbol{n}\cdot\left[\tilde{\boldsymbol{r}}_E\left(t\right) - \tilde{\boldsymbol{r}}_E\left(t_0\right)\right] + \phi_{star}\left(t\right) \tag{18}$$

where

$$\phi_{star}\left(t\right) = \begin{cases} \dfrac{f_s T_s}{2c}\displaystyle\sum_{k=1}^{j-1}\left(\boldsymbol{n}^T\hat{\boldsymbol{v}}_{SC/E,k} + \boldsymbol{n}^T\hat{\boldsymbol{v}}_{SC/E,k+1}\right) & t = jT_s \\[2ex] \dfrac{f_s T_s}{2c}\displaystyle\sum_{k=1}^{j-1}\left(\boldsymbol{n}^T\hat{\boldsymbol{v}}_{SC/E,k} + \boldsymbol{n}^T\hat{\boldsymbol{v}}_{SC/E,k+1}\right) & t \in \left[jT_s \quad (j+1)\,T_s\right] \\[2ex] \quad + \dfrac{f_s}{2c}\left(t - jT_s\right)\left(\boldsymbol{n}^T\hat{\boldsymbol{v}}_{SC/E,j} + \boldsymbol{n}^T\boldsymbol{v}_p\right) \end{cases} \tag{19}$$

and $j = 0, 1, 2, \cdots\cdots, N - 1$.

4.2.2. *Removal of the orbital effect within the recorded photon TOAs.*   As illustrated in Section 3.2, the epoch folding operates on the premise that the investigated signal is of constant frequency. This subsection will show how to remove the time-varying orbital effect within the recorded photon TOAs and to have photon TOAs with a constant frequency.

Equation (18) can be rewritten as

$$\frac{1}{f_s}\phi_{\det}\left(t\right) - \frac{\phi_0}{f_s} = t - t_0 + \frac{1}{c}\boldsymbol{n}\cdot\left[\tilde{\boldsymbol{r}}_E\left(t\right) - \tilde{\boldsymbol{r}}_E\left(t_0\right)\right] + \frac{1}{f_s}\phi_{star}\left(t\right) \tag{20}$$

Setting $\bar{t} = \phi_{\det}\left(t\right)/f_s$ and $\bar{t}_0 = \phi_0/f_s$, we have

$$\bar{t} - \bar{t}_0 = t - t_0 + \frac{1}{c}\boldsymbol{n}\cdot\left[\tilde{\boldsymbol{r}}_E\left(t\right) - \tilde{\boldsymbol{r}}_E\left(t_0\right)\right] + \frac{1}{f_s}\phi_{star}\left(t\right) \tag{21}$$

Assuming there are M photon TOAs recorded within an observation period of a pulsar, the photon TOAs series is denoted as $\{t_i\}_{i=1}^{M}$. When Equation (21) is applied to all the photon TOAs, the orbital effect within $\{t_i\}_{i=1}^{M}$ can be roughly removed, bringing in new photon TOAs, $\{\bar{t}_i\}_{i=1}^{M}$. Compared with $\{t_i\}_{i=1}^{M}$, the period of $\{\bar{t}_i\}_{i=1}^{M}$ is the intrinsic period of the pulsar, i. e., $1/f_s$. Thus, the initial phase of $\{\bar{t}_i\}_{i=1}^{M}$ can be readily estimated by the classical epoch folding methods.

4.3. *Summary of the integrated pulse phase estimation method.*   The proposed integrated pulse phase estimation method can be complemented by the following procedure:

Step 1 Estimate the velocity of the vehicle at each sampling period of the starlight Doppler measurements according to Equation (10);

Step 2 Remove the orbital effect in the photon TOAs $\{t_i\}_{i=1}^{M}$ using Equation (21), and obtain $\{\bar{t}_i\}_{i=1}^{M}$;

Step 3 Calculate the initial phase of $\{\bar{t}_i\}_{i=1}^{M}$ using epoch folding methods.

5. SIMULATIONS.

5.1. *Simulation conditions.*   Three Earth orbiting satellites are investigated, and the initial elements of the three satellites are shown in Table 1. The pulsar PSR B1821-24 with parameters listed in Table 2 is employed as the observed pulsar. The template of PSR B1821-24 is given in Figure 5 (Rutledge et al., 2004). The ephemeris DE405 is employed to predict the position and velocity of Earth within the observation period of the pulsar. The fast-near maximum likelihood estimator is used to estimate the initial phase.

The sampling period of starlight Doppler measurement is 0·1 s and the measurement accuracy is 0·1 m/s. The navigation stars, the data of which is taken from Liu et al. (2015), are listed in Table 3.

Root Mean Square (RMS) error is selected to evaluate the initial phase estimation result. The phase estimation results are obtained from 1000 Monte Carlo trials.

5.2. *Hardware-in-loop system validation.*   The simulations are performed by the newly-developed hardware-in-loop system. Figure 6 provides a block diagram of the hardware-in-loop system. As a vehicle-borne experiment is difficult to perform, it is an effective and economical way to develop a hardware-in-loop system to simulate the actual space mission and to analyse the performance of the proposed integrated navigation system.

The system is mainly constituted of the following parts:

(1) X-ray signal simulation portion: Generate the X-ray photons according to the nominal orbital information of the investigated vehicle, and detect the photon TOAs by employing a Silicon Drift Detector (SDD).

   It is worth noting that the generation and detection of the X-ray photons are performed in a vacuum pipeline with a length of 3 m, as the X-ray radiation would rapidly attenuate in the atmosphere.

(2) Starlight Doppler measurement simulation computer: Simulate the starlight Doppler measurement according to the nominal orbital information of the investigated vehicle as well as the ephemeris of the observed stars.

(3) Fusion unit: perform the proposed integrated pulse phase estimation method to estimate the pulse TOA.

(4) High-fidelity orbital dynamics simulation computer: Simulate a high-fidelity space dynamics environment to provide the nominal orbital information to the starlight Doppler measurement simulation computer and the X-ray signal simulation portion.

(5) Integrated navigation simulation computer: Calculate the position and velocity of the investigated vehicle using the pulse TOA provided by the fusion unit.

Table 1.   Initial orbital elements of satellites.

Orbital elements	Satellite 1	Satellite 2	Satellite 3
Semi-major axis [km]	10027·37	26570·08	42199·55
Eccentricity	0·003	0·047	0·0015
Inclination [°]	68·75	63·15	10·44
Right ascension of the ascending node [°]	174·21	136·31	322·41
The argument of perigee [°]	351·09	211·64	201·63
Mean perigee [°]	2·15	44·16	184·45

Table 2.   Parameters of Simulated PSR B1821-24.

Item	Value
Period [ms]	3·05
α [ph/s]	1·93
β [ph/s]	50
Initial Phase [cycle]	0·4
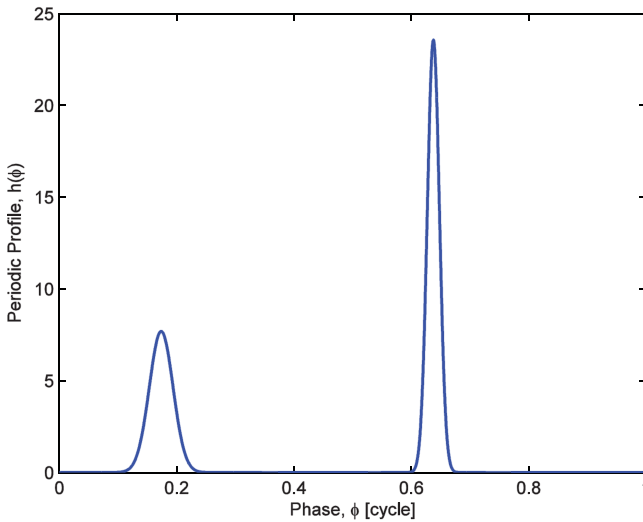
Figure 5.   PSR B1821-24 profile.

Table 3.   Navigation stars.

Star	Sirius	Canopus	Arcturus
Right ascension [°]	101·29	95·99	213·92
Declination [°]	−16·72	−52·70	19·18

As the key portion of the integrated navigation system is the fusion unit, we will first analyse the performance of the integrated pulse phase estimation method.

Figure 7 shows the phase estimation result of the proposed method for the three satellites. For the three satellites, the RMS errors of estimated phase all reduce as the observation period of a pulsar increases. When the observation period is less than a threshold of around
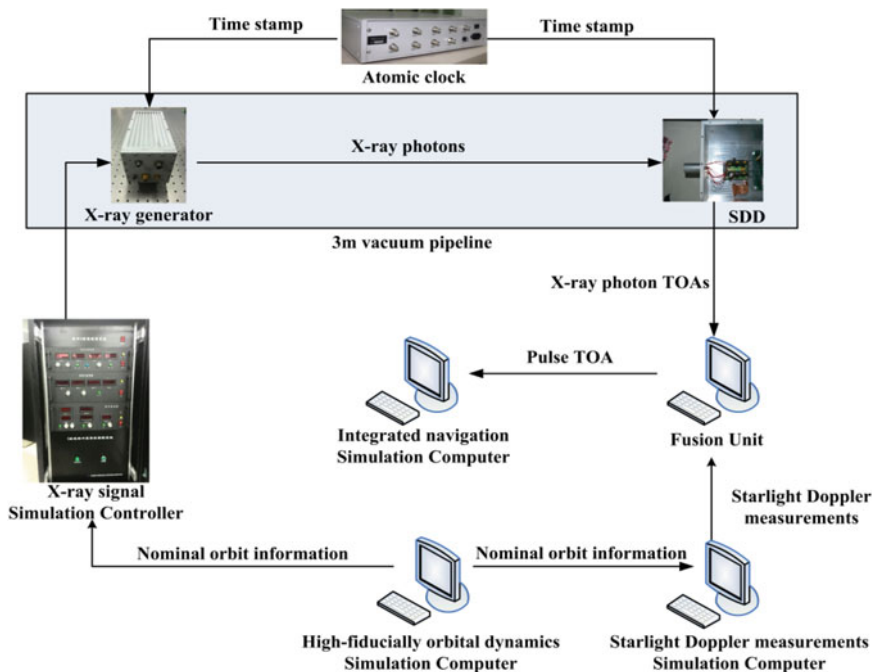
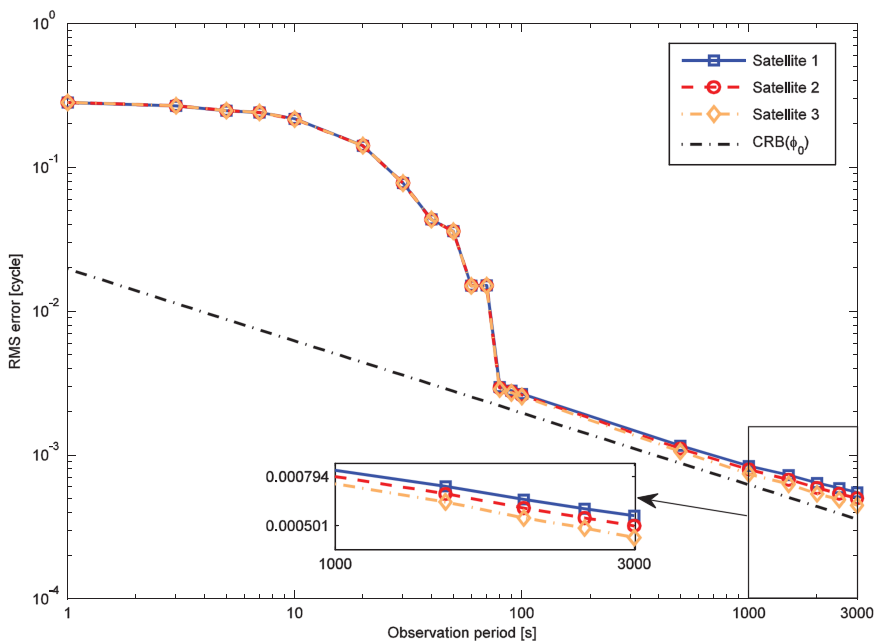Figure 6.   Block diagram of the hardware-in-loop system.

Figure 7.   Initial phase estimation results for three satellites.
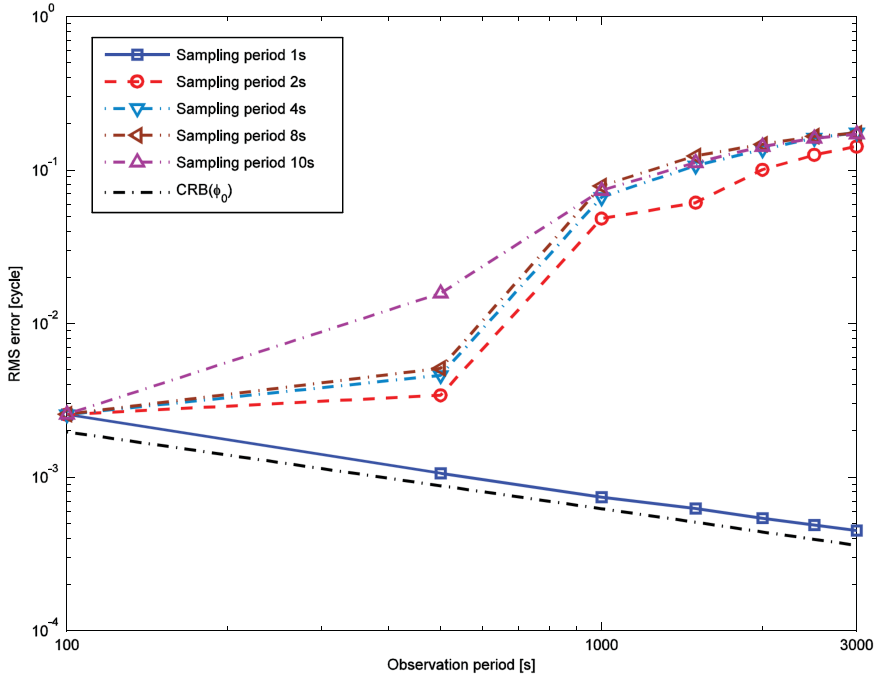
Figure 8.   RMS error of initial phase with different sampling periods of the starlight Doppler measurement.

100 s, the RMS errors experience an unreliable region, and the phase estimation result should not be used. When the observation period exceeds the threshold, the RMS errors become linearly convergent to the Cramér-Rao Bound (CRB) and finally reach an accuracy of about 0·001. This means the proposed method could effectively reduce the orbital effect. In addition, the estimation accuracy grows as the orbital altitude of the satellite increases. Thus, we will first select satellite 1 to analyse the factors that might affect the performance of the proposed method.

Figure 8 shows the pulse phase estimation results with different sampling periods of starlight Doppler measurements. As the observation period shorter than 100 s is the unreliable region, Figure 8 merely provides the results when the observation period is greater than 100 s. When the sampling period is greater than 1s, the RMS error curves all diverge from the CRB. This is because the sampling period growth is accompanied with an increasing approximation error of the satellite orbit. As Equation (17) showed, the velocity of the satellite within the sampling period is calculated by linearly interpolating. In other words, the orbit of the satellite is assumed as a line within a sampling period of starlight Doppler measurement. The sampling period continuing to grow would violate the assumption, bringing in an error impossible to ignore. Thus, in order to have a reliable pulse phase estimation result, the sampling period of starlight Doppler measurement should not be longer than 1 s.

Assuming the sampling period of starlight Doppler measurement is 1 s, Figure 9 displays the pulse phase estimation results with different starlight Doppler measurement accuracies ranging from 0·1 m/s to 1 m/s. All the RMS error curves converge to the CRB as the observation period increases, and the difference among the RMS error curves is slight. This means the accuracy of the starlight Doppler measurement puts little impact on the pulse
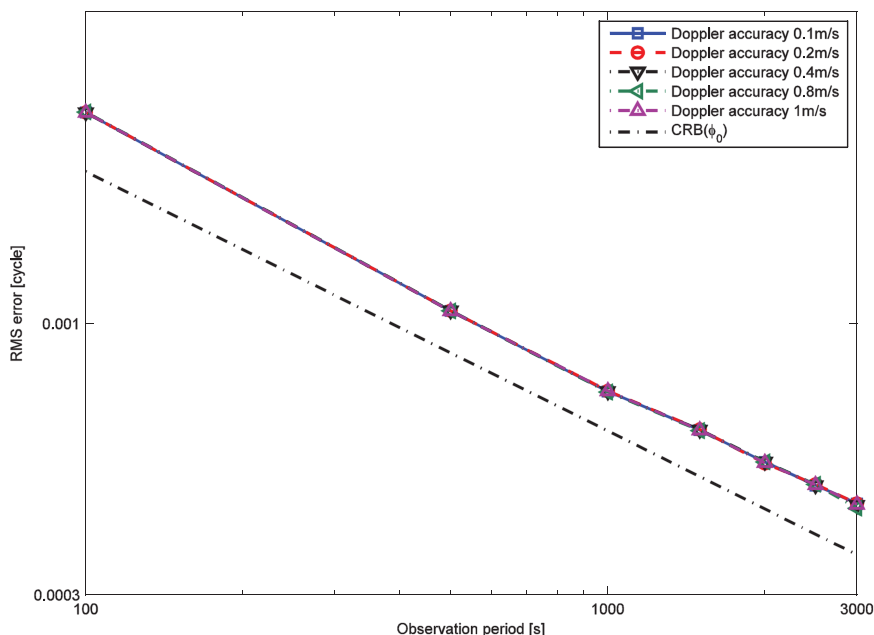
Figure 9.   RMS error of initial phase varying with the starlight Doppler measurement accuracy.

phase estimation. Thus, the proposed method drops the requirement of the accuracy of starlight Doppler measurement and a device with an accuracy of 1 m/s is sufficient.

Next, we compare the performance of the proposed integrated phase estimation method to the linearized method. As shown, for the satellites with orbit altitude of higher than 28,000 km (e.g. satellite 3 in this section), the order of the polynomial component of the linearized phase propagation model should at least be 2. In order to make a simple performance comparison, we use satellite 3 to perform the comparison.

Figure 10 compares the phase estimated by the proposed method and that estimated by the linearized method. Both methods converge to the CRB as the observation period increases. The phase estimation results are close to each other. In the simulation environment that contains Intel I7-4710MQ@2·5 GHz and Visual studio 6·0, Figure 11 compares the CPU time cost by the two methods. The linearized method is performed using the 10-threads parallel computation technique and the proposed method is performed using only one thread. Even if the linearized method employs the parallel computation technique, the integrated phase estimation method expends much less CPU time than the linearized method. Thus, the integrated pulse phase estimation method could achieve a phase estimation result similar to the linearized method but requires much less computational complexity.

Finally, we investigate the navigation performance of the proposed integrated navigation system. Besides PSR B1821−24, PSR B0540−69, and PSR B0531+21 are adopted. Satellites 1, 2, and 3 are all investigated, and the initial position and velocity error of the satellites are set to be 1 km and 1 m/s along each axis in the Earth-centred Inertial Coordinate System J2000·0. The investigated satellites are assumed to sequentially observe the three pulsars for 1,800 s to perform navigation.
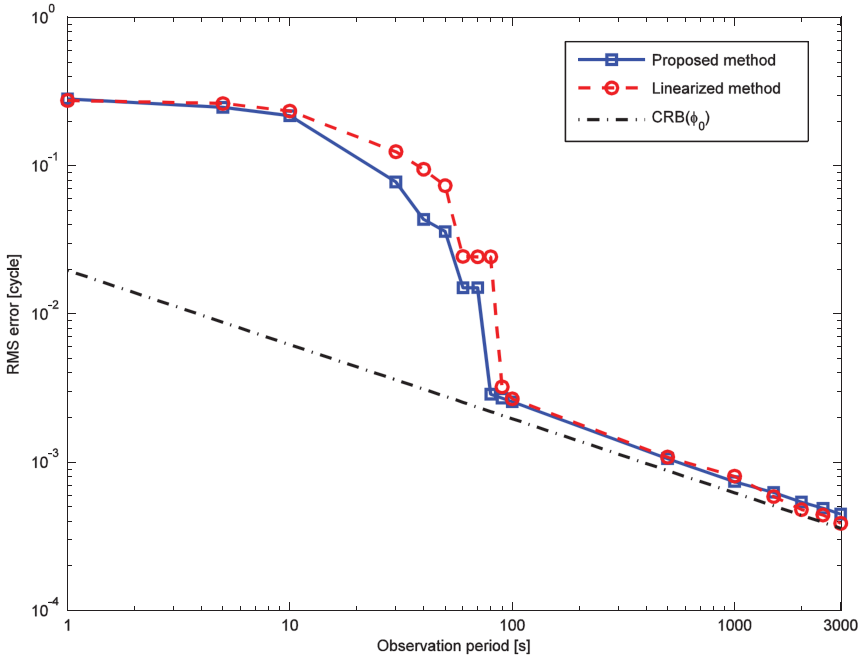
Figure 10.   Initial phase estimation result of the integrated phase estimation method and of the linearized method.
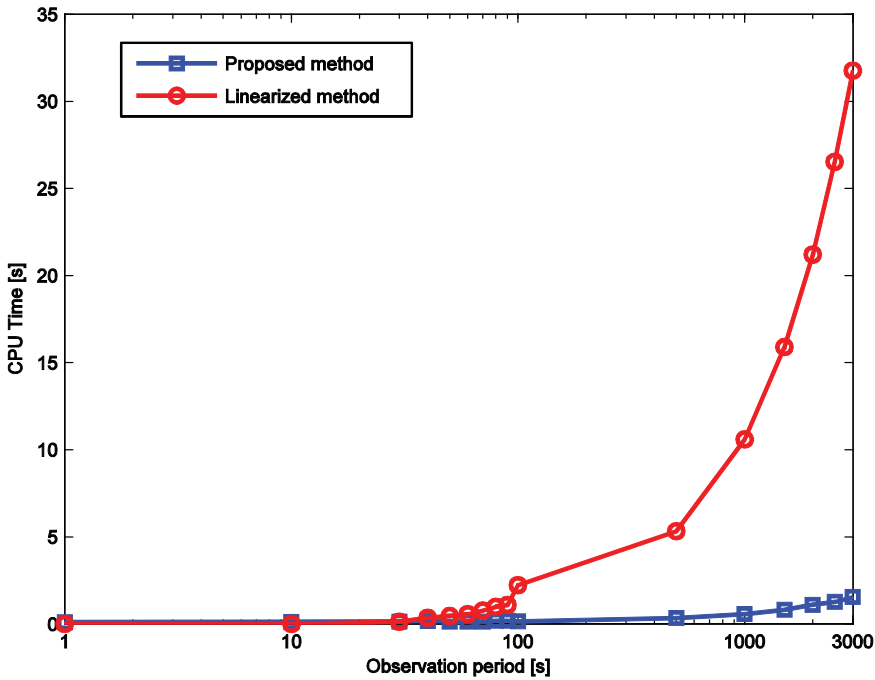

Figure 11.   The CPU time cost by the integrated phase estimation method and by the linearized method.
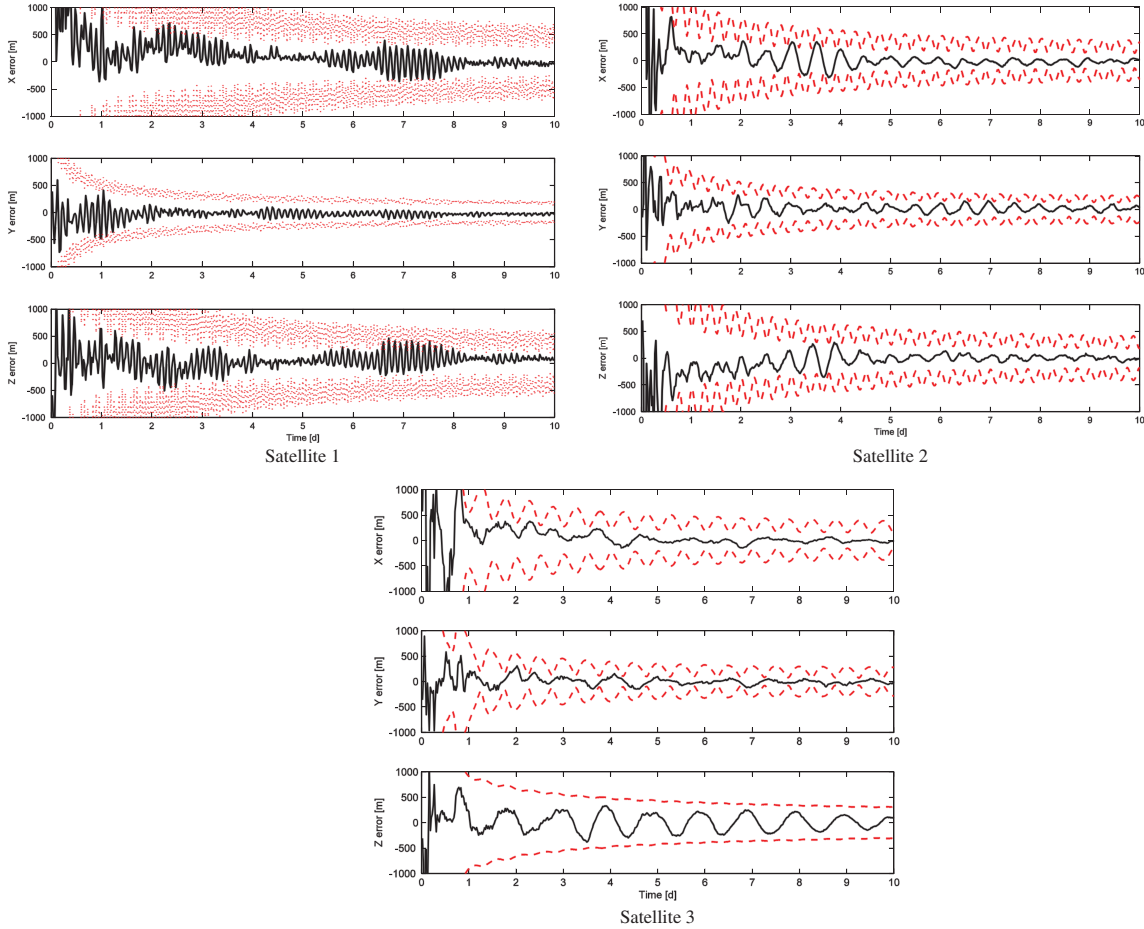
Figure 12. Positioning performance of the integrated navigation method.

Figure 12 shows the positioning results of the three satellites. The solid lines represent the positioning errors and the dashed lines denote the 3σ outlines. The positioning errors of the three satellites are all within the 3σ outlines, indicating that the proposed integrated navigation method could guarantee a reliable positioning result. As the integrated pulse phase estimation method could save computation resource, the corresponding integrated navigation method is promising.

6. CONCLUSIONS.   An X-ray pulsar/starlight Doppler deeply-integrated navigation method is proposed in this paper. In order to reduce the computational complexity of the current pulse phase estimation method for orbiting vehicles, a starlight Doppler measurement is introduced into the pulse phase propagation model to remove the orbital effect within the recorded photon TOAs and to convert the original photon TOAs with a time-varying unknown frequency into photon TOAs with the intrinsic frequency of the pulsar. Then, the pulse phase can be estimated by well-developed and computationally efficient epoch folding methods. Given that only the pulse phase needs to be estimated, the integrated phase estimation method expends little computation resource and is suitable for orbiting vehicles. Taking three Earth-orbiting satellites for examples, some simulations are performed by the newly-developed hardware-in-loop system. The results have shown the integrated pulse phase estimation method is applicable to various vehicles with orbital altitude ranging from 3,000 km to 38,000 km, is capable of handling the signals from millisecond pulsars, the fluxes of which are extremely faint, and costs a much smaller computation burden than the existing pulse phase estimation methods for orbiting vehicles. In addition, the corresponding integrated navigation system could provide reliable positioning results.

REFERENCES

Becker, W., Werner, M., and Jessner, A. (2013). Autonomous Spacecraft Navigation with Pulsars. *arXiv preprint arXiv: 1305.4842*.

Emadzadeh, A., and Speyer, J. (2011). *Navigation in space by X-ray pulsars,* Springer Press.

Emadzadeh, A., and Speyer, J. (2010a). On modelling and pulse phase estimation of X-ray pulsars. *IEEE transactions on signal processing*, **58**, 4484–4495.

Emadzadeh, A., and Speyer, J. (2010b). X-ray pulsar-based relative navigation using epoch folding. *IEEE transactions on Aerospace and electronic systems*, **47**, 2317–2328.

Golshan, A., and Sheikh, S. (2007). On pulse phase estimation and tracking of variable celestial X-ray sources. *Presented ION 63rd meeting*.

Liu, J., Fang, J.C., Ma, X., Kang, Z.W. and Wu, J. (2015). X-ray pulsar/starlight Doppler Integrated Navigation for formation flight with ephemerides errors. *IEEE Aerospace and Electronic Systems Magazine*, March, 30–39.

Lyne, A. and Craham-Smith, F. (2012). *Pulsar astronomy*, Cambridge University Press.

Ning, X.L. and Fang, J.C. (2007). An autonomous celestial navigation method for LEO satellite based on unscented Kalman filter and information fusion, *Aerospace Science and Technology*, **11**, 222–228.

Rinauro, S., Colonnese, S. and Scarano, G. (2013). Fast near-maximum likelihood phase estimation of X-ray pulsars, *Signal Processing*, **93**, 326–331.

Hildebrand, F. (1974), *Introduction to numerical analysis*, 2nd edition, McGraw-Hill.

Rutledge, R., Fox, D., Kullkarni, S., Jacoby, B., Cognard, I., Backer, D. and Murray, S. (2004). Microsecond timing of PSR B1821-24 with Chandra/HRC-S. *Astrophysics Journal*, **613**, 522–531.

Sala, J., Paredes, J., Urruela, A., Estalella, R. and Villares, X. (2004). *Feasibility Study for A Spacecraft Navigation System Relying on Pulsar Timing Information*. ARIADNA Study 03/4202.

Sheikh, S.I., Pines, D.J., and Ray, P.S. (2006). Spacecraft Navigation using X-ray Pulsars. *Journal of Guidance, Control and Dynamics*, **29**, 49–63.

Tran, N., Renaux, A., Boyer, R., Marcos, S. and Larzabal, P. (2014). Performance bounds for the pulse-phase estimation of X-ray pulsars, *IEEE transaction on Aerospace and electronic systems*, **50**, 786–794.

Wang, Y.D. and Zheng, W. (2016). Pulse phase estimation of X-ray pulsar with the aid of vehicle orbital dynamics. *Journal of Navigation*, **69**, 414–432.

Wang, Y.D., Zheng, W., Sun, S.M. and Li, L. (2013). X-ray pulsar-based navigation system with the errors in the planetary ephemerides for Earth-orbiting satellite. *Advances in Space Research*, **51**, 2394–2404.

Wang, Y.D., Zheng, W., Sun, S.M. and Li, L. (2014). X-ray pulsar-based navigation using time-differenced measurement. *Aerospace Science and Technology*, **36**, 27–35.

Winternitz, L.M.B., Hassouneh, M.A. and Mitchell, J.W. (2015). X-ray pulsar navigation algorithms and testbed for SEXTANT, *Technical Report to NASA*.

Yang, W. B, Li, S.Y. and Li, N. (2014). A switch-mode information fusion filter based on ISRUKF for autonomous navigation of spacecraft, *Information Fusion*, **18**, 33–42.

Yim, J. (2002). Autonomous spacecraft orbit navigation. PhD Thesis, Texas A&M University, 2002.